Integrated Optical Cavities

Tadeas Liska

May 3, 2013

Abstract

Spintronics is an emerging field with numerous applications including quantum computing of which a key component is the ability to monitor the spin state of a system. Such monitoring can be achieved optically using spin-photon interactions such as the Faraday rotation. Optical cavities provide an approach to enhancing the efficiency of such measurements by exploitation of the Purcell effect. We have simulated photonic crystals in the form of distributed Bragg reflectors (DBR) consisting of alternating layers of SiO_2 and TiO_2 using the MEEP simulation environment and transfer matrix calculations. By destroying the symmetry of our structure through the incorporation of a defect we show that this leads to a normal mode at 600nm. Subsequently we have begun the fabrication of our resonant crystal with an optimized design of fourteen stacks determined by harmonic analysis of the simulations. Additionally, we plan to incorporate CdSe/ZnS core-shell quantum dots (QDs) in the defect layer so as to be able to initialize a spin density through optical pumping and observe the Faraday rotation of a linearly polarized pulse. The Bragg reflector cavity is being constructed in the MORE center using electron beam physical vapor deposition and radio frequency magnetron sputtering. Once complete it will be tested in the Berezovsky lab, measuring parameters such as the cavity Q-factor, Purcell factor enhancement, and Faraday rotation.

Contents

List of Figures

Chapter 1

Introduction

1.1 History

Quantum mechanics has fundamentally changed most of physics and revealed grand underlying causes to macroscopic events so it is of no surprise that in the world of optics this trend continues. The aptly named field of quantum electrodynamics (QED) concerns itself with the interactions between light and matter at the atomic level and is built up from the notion of modeling light as a superposition of modes of harmonic oscillators. Successes from this theory include the description of spontaneous and stimulated emission to the proposition of superconducting circuits.[1] Naturally, it was but a matter of time before optical cavities were to be studied under this framework. Cavity quantum electrodynamics (cQED) has at its heart the Jaynes-Cummings model which describes the interactions that a two-level system undergoes with a resonant mode of a cavity. Since an electron in a quantum dot can be approximated as a two-level system the Jaynes-Cummings model is appropriate and proposes a Purcell factor which relates the emission rate of an electron in space to that within a resonator. This Purcell enhancement has

been used to mitigate the observation of quantum effects in the laboratory by enhancing signals proportional to a cavity's quality factor. That Faraday effect, though first understood by its namesake without the use of quantum mechanics, has also had its origins elucidated as the magnetic coupling of light to spin.

1.2 Background & Aims

To date, a significant challenge in the world of optics has been the ability to measure spin-photon coupling to non-negligible accuracy.[2] Previous efforts have been able to demonstrate that a viable approach to this problem includes the use of optical cavities that have finely-tuned resonances and broad band gaps.[3] By embedding quantum dots (QD) the structures exploit the Purcell effect to elicit an enhancement in the coupling strength and consequently produce coherent spin states. A common design for an optical cavity is a distributed Bragg reflector (DBR), which consists of alternating layers of materials with differing indices of refraction sandwiching a thicker layer of the low refractive index material. The thicker layer acts as a defect in an otherwise periodic structure and results in the presence of a normal mode. Without it the structure simply acts as a stop-band filter around some center frequency. The resonant frequency of such a structure can be selected by varying the film thickness and specific geometries can give especially good fidelity in terms of isolating the transmission of that frequency.[4] The aim of this project is to construct one such integrated microcavity and indirectly monitor the decay of the spin state of the QDs.

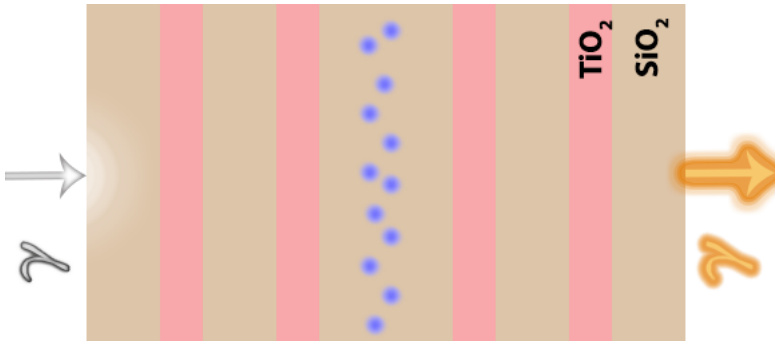

Figure 1.1: Author's conception of DBR cavity with embedded CdSe/ZnS QD's

To this end, the following set of objectives has been devised:

- Simulation of DBR microcavity using the MEEP framework
- Fabrication of SiO_2/TiO_2 DBR microcavity using a combination of electron beam chemical vapor deposition and radio frequency ion sputtering
  - Embedding of CdSe/ZnS core-shell Quantum Dots
- Characterization of DBR microcavity through spectroscopic ellipsometry and stylus profilometry
- Testing of the integrated microcavity in the Berezovsky lab, determining such parameters as the Q-factor, Purcell enhancement, and Faraday rotation

1.3 Motivation

The immediate results of this experiment will give insight into the relaxation dynamics of a spin-pumped system. It is an exceptionally difficult matter to determine the spin-state of an electron without continuous measurement, which would effectively void the role of such a measurement altogether. By inducing a change in rotation of linearly polarized light as it passes through a material we can indirectly gain information about

the underlying cause of said rotation which, in this case, would be the presence of a spin-polarization. This piece of information is useful as a principal component of future spintronics research. The eventual goal of spintronics is to develop a quantum analog to a digital computer with information and logic being carried out by spin-state operations rather than the conventional voltage gating. Naturally before we can devise methods of imprinting data to a spin-state and at a later time extracting new data we need to understand how spin-states evolve in time and how we are to measure them. The optical cavity, with its Purcell enhancement, is a prime candidate for at least the measurement of a spin-state.

1.4 Methods

The primary tools used in this project are the MEEP simulation environment and an Angstrom deposition system. The MEEP environment, interfaced with through the Scheme interpreter, allows for a large number of simulations with varying parameters to be explored. The limitation to these simulations is that, at the level scripted, they provide information solely on the transmission spectrum of a structure. As such, the task laid out for this portion of the project is to determine optimal values for parameters such as thickness and number of stacks before beginning the fabrication phase.

The Angstrom deposition system is a composite of an ultra-high vacuum chamber, electron beam physical vapor deposition (e-beam PVD), and ion sputtering functionalities. During operation the chamber is kept on the order of 10^{-6} Torr and the deposition is monitored via dedicated quartz crystals. A project specific process was written into the system's interface consisting of an initial layer of silica to be deposited by e-beam PVD followed by a titania layer deposited through radio frequency (RF) ion sputtering. Be-

fore deposition the system was calibrated for both materials so as to ensure reproducible accuracy in terms of layer thickness.

The middle cavity of silica is also deposited using e-beam PVD but to embed the quantum dots within it requires treatment with perhydropolysilazane. This inorganic polymer consists of alternating S-N bonds with valance completing hydrogens instead of organic moieties. Upon interaction with moisture, in the air for instance, the material liberates ammonia and leaves behind an inorganic amorphous silica layer. By solvating the QD's in the polysilazane colloid and spin-coating them on a preliminary layer of silica we can integrate a layer with embedded quantum dots before depositing up to the required final thickness of the cavity.

In the lab we can now investigate the Faraday rotation and Purcell factor of our constructed cavity. By viewing the rotation of the transmitted light, with reference to a known linearly polarized source, we can extract data regarding the density of excited states. To establish a coherent spin-polarization it is necessary to rapidly alternate between a circularly polarized pump and linearly polarized probe pulse. The pump is expected to excite electrons within the QD's and thus generate a polarization across the layer in which they are embedded. Faraday rotation is observed when photons interact magnetically with a spin field, experiencing an alignment rotation proportional to the magnitude of the spin polarization. As such a larger density of excited quantum dots within the cavity should produce the highest rotation right after the pump pulse and decay down to a relaxed state with no observed rotation in transmitted light. Such a measurement gives us indirect knowledge of the relaxation dynamics of an electron after its state has been initialized. Additionally, due to the support that the resonance mode encounters in the defect layer the light remains contained long enough to be absorbed

by the QDs and summarily remitted resulting in a coupling between them and the defect layer. This results in a Purcell effect which enhances the spontaneous emission of radiation within the cavity leading to multiple internal reflections and an increase in the coherence of the initialized spin-states.

1.5 Results

Over the course of one year a great deal of information regarding photonic crystals has been absorbed and likewise produced. First, we have discovered that the MORE center Angstrom system required tinkering to make the deposition of titania feasible. As a result a secondary support has been constructed that increases the efficiency of the system by six-fold through a reduction in target-substrate separation. In terms of the computational portion of this project we have successfully used MEEP and its associated Harminv package to examine the cavity's normal mode fidelity as a function of number of stacks. We have found that at fourteen stacks we see the highest quality factor, near 2000, and successive addition of stacks amounts to marginal differences. Furthermore, a transfer matrix program was used to verify the behavior of the proposed structure and both the stop-band and resonance were observed. Finally, despite a malfunction halting production the Angstrom system has been calibrated for use on both materials and stacks had begun to be deposited with an overall accuracy of 6%.

Chapter 2

Theory

2.1 Optical Cavities

To fully comprehend how the optical cavity retains a normal mode within a stop-band filter we have to borrow tools from solid state theory and QED. First, let us consider only the photonic crystal as a DBR, without the center defect cavity, and following that we will introduce the defect and see how that changes our physics. As our cavity has a periodicity in one direction, let's say that this is the z-direction, we can write the allowed modes in Bloch form:

$$H_{n,k_z,\mathbf{k}_{||}}(\vec{\mathbf{r}}) = e^{\imath \mathbf{k}_{||} \cdot \rho} e^{\imath k_z z} \mathbf{u}_{n,k_z,\mathbf{k}_{||}}(z) \tag{2.1}$$

Here we have $\mathbf{k}_{||}$ as the wave vector in the plane, k_z as the wave vector in the z-direction, and n as the band number or index of the mode. Additionally, $\mathbf{u}(z)$ is periodic such that $\mathbf{u}(z) = \mathbf{u}(z + R)$. From our description of the crystal it is clear that there is translational symmetry in the xy-plane, and thus $\mathbf{k}_{||}$ can take any value. By a similar argument k_z is restricted to certain values, namely those within the Brillouin zone. If we denote the primitive lattice vector in the $\hat{\mathbf{z}}$ direction with magnitude a, then the primitive

reciprocal lattice vector is $\frac{2\pi}{a}\hat{\mathbf{z}}$ and we recover the following condition restricting k_z:

$$\frac{-\pi}{a} < k_z \leq \frac{\pi}{a} \tag{2.2}$$

Now, considering only light in the $\hat{\mathbf{z}}$ we can apply this condition to each layer and we notice that the two frequencies as a result do not match! This is due to the fact that in a medium the frequency of a mode is a quotient of the refractive index. So in each of the layers, since they have different refractive indices, some of the wavelengths will fall outside the Brillouin zone and not satisfy our boundary conditions.[5] As a result they are suppressed and decay evanescently into the structure.

The resulting band gap is determined by the contrast of the two refractive indices, a larger contrast garners a larger band gap. A common characterization of these photonic band gaps is the gap-midgap ratio which is independent of scale and defined as $\frac{\Delta\omega}{\omega_m}$.[5] We quantify this relationship in the approximation $\frac{\Delta\epsilon}{\epsilon} < 1$ as follows:

$$\frac{\Delta\omega}{\omega_m} \approx \frac{\Delta\epsilon}{\epsilon}\frac{\sin(\frac{d\pi}{a})}{\pi} \tag{2.3}$$

This equation can be seen to have a maximum when $d = 0.5a$ but that is only valid within our approximation. For a more detailed treatment see Yeh(1988) in which he derives that the gap-midgap ratio is maximized for quarter wavelength stacks of each of the materials.[6] The physical interpretation of this result is that at each material interface the reflected waves are in phase and destructively interfere, enhancing their suppression.

Having describing the on-axis propagation of our photonic crystal let us now incorporate a defect, of the lower ϵ material, in the center of the structure. We have now broken the one-dimensional symmetry of our crystal and as a result a localized mode can exist with some lifetime within the defect layer. Since we have enclosed this mode within two layers of high refractive index material it will bounce back and forth and thus

be sustained for some time. This, in essence, is related to the cavity quality factor as a coherent mode will last longer than one that is broadly defined.[7] We have constructed our defect as a half wavelength thick layer, for a resonance at 600nm, but we can increase or decrease the wavelength by adjusting this thickness as it is simply a matter of the mode being spatially confined.[5]

2.2 Purcell Effect

In the mid-1900's there was much concern in the physics world about the quantum nature of light and the phenomenon of radiation. Then in 1932 Enrico Fermi published his Quantum Theory of Radiation in which he generalized Dirac's quantum theory of radiation and introduced QED.[8] In this scheme he uses Dirac's electron wave function, which incorporates spin to derive the Hamiltonian, which will be spared due to size, for an atom within an electromagnetic(EM) field. In 1962, Jaynes and Cummings devised their model of an atom, termed an emitter, within a resonant cavity. The Jaynes-Cummings model was used to determine the relationship between the spontaneous emission of an emitter in vacuum to that within a homogeneous medium, such the defect layer in our experiment.[9] What they discovered was a significant increase in the spontaneous emission probability as compared to an emitter in a vacuum. Specifically, for a lossless cavity the interaction time is on the order of tenths of a second, whereas in vacuum it is of order 10^{-7}.[9] Before the time of its publication many developments had been made in connecting abstract mathematical fields to quantum mechanics that allowed them to elegantly arrive at this result by a simple approximation and the solving of a quadratic equation. Their procedure consists of finding the probability of emission or absorption in the interaction Hamiltonian and focusing on the case where the cavity resonant frequency

is tuned to the energy separation between a two-level emitter. This enhancement in spontaneous radiation falls out naturally from Fermi's golden rule and is termed the Purcell enhancement.[10] The following equations illustrate the difference between emission in vacuum, Γ_0 and in a resonant cavity Γ_{cav}:

$$\Gamma_0 = \frac{\omega^3}{3\pi\hbar c^3}\frac{|D_{ef}|^2}{\epsilon_0} \tag{2.4}$$

$$\Gamma_{cav} \approx \Gamma_0 \frac{Q\lambda^3}{V} \tag{2.5}$$

Here we note that D_{ef} is the matrix element of the electric dipole of the emitter between its two levels, Q is the cavity quality factor, and V is the volume of the cavity. It is apparent that the Purcell enhancement is proportional to $\frac{Q}{V}$ meaning that the geometry of the cavity is as important as its confinement capabilities. This is not entirely true as its quality itself depends on the geometry, which is a possible explanation of the Q-factor plateauing after 14 stacks. In situations when the cavity has exceedingly high fidelity, in the thousands, the ratio $\frac{|D|_{ef}}{\Delta\omega_m} > 1$ and the radiation remains inside the cavity for long enough so as to lead to a coupling between the emitter and the defect mode.[10] In this scenario spontaneous emission becomes reversible and the emitter exchanges energy at the cavity resonance analogous to Rabi oscillations. This very same concept is found in nuclear magnetic resonance except in this case the atom couples with its own one-photon field![10]

2.3 Faraday Rotation

Finally, the effect that we wish to measure in our experiment, the Faraday Rotation, was first discovered by Michael Faraday in 1845. By placing an isotropic dielectric in a uniform magnetic field he found that linearly polarized light, sent through the material,

experiences a rotation in its plane of polarization.[11] This rotation is proportional to the magnetic field magnitude and the linearly polarized light attempts to align with its net direction.

In the cavity we are constructing we hope to utilize the Purcell enhancement to maintain a density of spin comprised of the excited QD's. This way, we are simulating the magnetic field in Faraday's experiments. Since the construction of the QD's is such that the electrons are confined spatially in its shells we expect that there will be a strong correlation among them in the direction their spin points. The actual initiation of this density is to be achieved by stimulation of a circular polarized pulse which would be followed by the linearly polarized probe pulse. As we have constrained the frequency of our interaction, namely the resonance frequency we expect to obtain a damped oscillating signal with one fundamental frequency in its Fourier spectrum.

Chapter 3

Simulation

3.1 MEEP

MEEP, an acronym for MIT Electromagnetic Equation Propagation, is an open-source software for Linux available from MIT that uses a finite-difference time domain (FDTD) method to evaluate the spatial and time derivatives of Maxwell's equations. In this setting we divide time and space into a grid of discrete points at which Maxwell's equations are approximated in a leap-frog scheme. In contrast to frequency domain methods carrying out these calculations in the time domain allows one to extract results for a range of frequencies rather than at a single frequency. This is achieved by carrying out the computations, in time, within frequency space by way of Fourier transform, whereas in frequency domain calculations we evaluate what happens to a signal of a given frequency over time. A FDTD method also allows for the evaluation of eigenfrequencies of a structure, a particularly useful calculation as we are searching for resonances in our project. This is incorporated into MEEP through the Harminv package which evaluates the Fourier components of in a specified region some time after the initial sources are

turned off. The output here is in the form of the modes that are sustained within the structure along with their respective quality factor.

3.1.1 Scheme vs. Python

The two main languages in which MEEP can be coded are Scheme and Python. The differences between the two are vast and start with the fact that Scheme is an interpreted language whereas Python is compiled. This is most evident in the way that they incorporate abstraction. In Python we have generic classes such as *dielectric* which can be customized according to position in the computational grid and will associate a dielectric value with each point in a specified region. Scheme, which is based on Church's lambda calculus, encapsulates abstraction by nesting methods. In this case we have a function called *block* which specifies a geometric figure in which we nest properties using parentheses. Everything in Scheme is contained in parentheses whereas Python uses white space to divide function calls. Since Python allows us to abstract and customize our classes and methods it gives higher-level control but the documentation on it is lacking in substance. Scheme on the other hand is a very low-level language and much of the intricacy associated with its methods is hidden to the programmer. However, since it is an interpreted language it relies solely on syntax and becomes very tedious to debug as it cannot localize an error. Scheme is read line-by-line and once it reaches a syntactic inconsistency, such as missing a parentheses, it will generate an error, regardless of where in the script it may appear. There are banes and boons to using each language; Scheme is more easily accessible as it reads like plain English whereas Python requires more programming savvy, but if one possess this savvy then Python is much more powerful. One extremely important distinction between the two is in the way that they define

their origins: Scheme takes the center of the grid as the origin and defines everything relative to that, whereas Python uses the upper left-hand corner as the origin. Initially I attempted to use Python but as stated before the documentation is limited and after being unable to decipher the method for defining a dielectric material I switched over to Scheme. Scheme allows for the scripting of one, two, and three dimensional problems but as our structure has one dimensional symmetry I wrote code for up to two dimensions.

3.1.2 Computational Environment

The three main components to any MEEP simulation whether coded in Python or MEEP are the definition of a computational grid and structure, instantiation of sources, and specifying flux regions. Excerpts for each along with explanations are provided below. Note

The first is easy enough in Scheme, being called using

```
(set! geometry-lattice (make lattice (size grid_x grid_y no-size)))
```

The command "set!" is used in any instance where a parameter or method is called. Notice the special value "no-size", which here dictates that we are working in two dimensions. Another such special value is "infinity" which is coded as a vary large number on the order of 10^{20} and is used when defining extremely large or non-existent dimensions. The distinction between the two is not great as "no-size" literally replaces the specified cells with a non-coded region whereas "infinity" sets them to a computationally irrelevant value. The two can and are used interchangeably when coding a simulation. As stated before, the parentheses act as surrogates for abstraction so the above example can be understood as first defining a region using "size", then making that a lattice, and finally setting it as a special type of lattice referred to as a geometric object in Scheme. The

lattice and geometric object "classes" are defined within the program and the user has no access to them.

MEEP supports structural definitions in Cartesian, spherical, and cylindrical coordinates in each case using the "list" or "append" functions to create a single structure composed of multiple parts. The distinction between the two is that "append" allows one to define structures within structures such as a hole in an otherwise uniform dielectric medium. Appendix A has an example script for a two-dimensional simulation in which one can clearly see how to go about defining dielectric materials in the computational grid. Note that in Scheme comments or un-read code is denoted by a semi-colon and it applies on a line-to-line basis.

Next, once the geometric objects in the simulation are defined we must create some source in the form of E, B, or J along with a specified direction x, y, or z. To fully define a source one needs to include this component, a type (i.e. Gaussian), a center frequency and width, and location. Additionally we can also define a size.

Finally, we must tell the program where we want to evaluate the fields for such things as transmission and reflection spectra. This is achieved by defining flux planes, or points if in one-dimension, at certain locations over specific frequencies.

3.1.3 Data Collection & Analysis

The data output from MEEP is either in the form of transmission/reflection spectra or harmonic modes depending on whether we use the Harminv package or not. In the former case the data has to be converted to a readable form, .dat, using

```
grep flux1: foo.out > foo.dat
```

before we can import it into MATLAB for processing. In order to normalize the data two simulations are run, one is a calibration which does not include the center defect, and the other is the experimental which does include the defect. Dividing these two data sets gives us the normalized results. When using Harminv the data is output after the simulation is run in a conveniently easy to read format: frequency, amplitude, and Q-factor.

3.2 Transfer Matrix

The other computational component to this project was the use of a transfer matrix (TM) program written in MATLAB by Brent Valle. Here Snell's law and the continuity equations are evaluated at each material interface. The inputs here are a computational structure, which is defined using material objects that have real and imaginary refractive indices for a range of wavelengths, a material library to reference, and a wavelength vector along which to evaluate the equations. The output is in the form of two objects, one which covers the two polarizations of light, s and p, and another which is their absolute value. Since the materials that were defined in this program were given only real values we retrieve only s-polarized information. This object stores data in the form of transmission and reflection spectra and is used to show the stop-band and resonance behavior of our photonic crystal.

3.3 Computational Results

We have used MEEP and TM calculations to verify and optimize our cavity design. From MEEP we have determined the quality factor as a function of number of stacks which

has led us to optimize our design at 14 stacks. This was done by running Harminv on a series of simulations that varied the number of stacks the results of which appear below in Figure 3.1. Additionally, we have verified the band-gap features and the expected resonance using the TM program, displayed in Figure 3.2

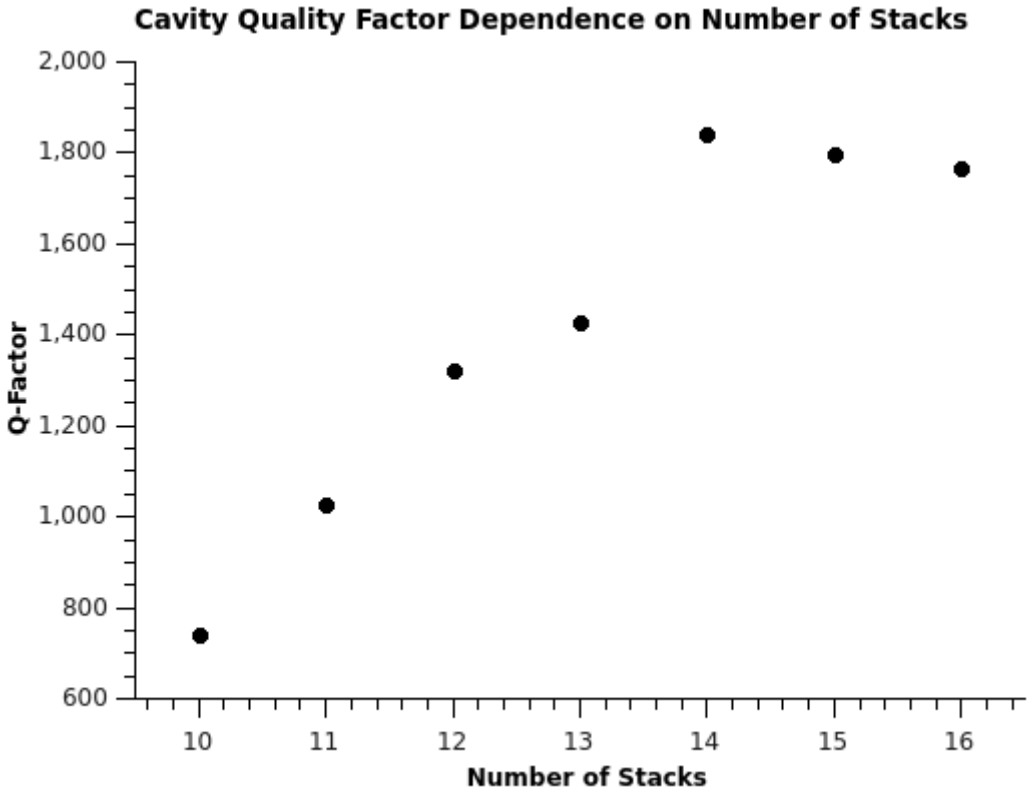

Figure 3.1: MEEP Harmonic Mode Analysis when number of stacks is varied

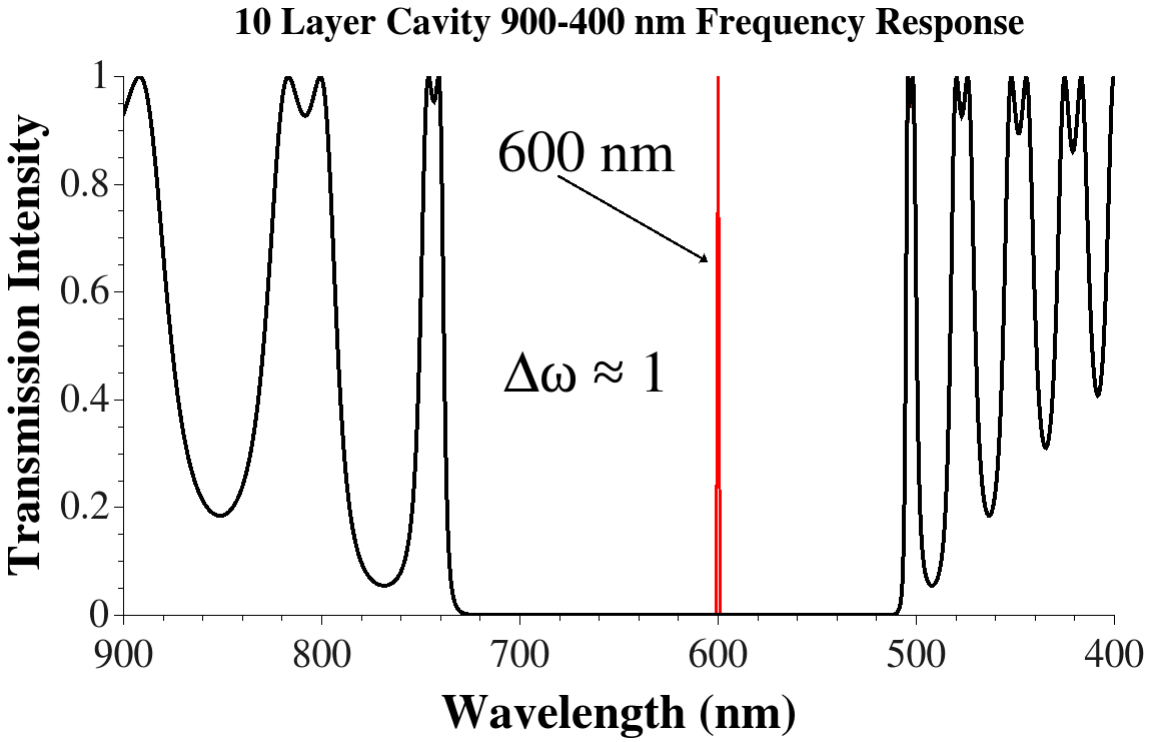

Figure 3.2: Transfer Matrix Output for 10 layer cavity. Resolution restricted to 1nm.

Chapter 4

Fabrication

4.1 Methods and Instrumentation

The MORE center on the 6^{th} floor of the White building provides a number of tools that we use to build our photonic crystal. It is equipped with an Angstrom® deposition system that possess a number of functionalities: electron beam physical vapor deposition (e-beam PVD), magnetron sputtering, and thermal evaporation stations.

For our project we have utilized the e-beam PVD pockets and the radio frequency (RF) magnetron sputtering assembly; Silica was deposited using e-beam PVD while titania was sputtered off a TiO_2 target. In both cases the substrate, a quartz slide, onto which we are depositing is suspended 9" above the targets held in place on a circular stage using screws. There is room for three slides on the platform and the majority of depositions that were done were in triplicate unless otherwise noted. A shutter covers the substrate until the targets have completed an initial ramp and a steady deposition rate is observed by the quartz crystals. We would like to deposit these two materials at the desired thicknesses consistently and in a timely manner. We have planned to deposit fourteen layers of each

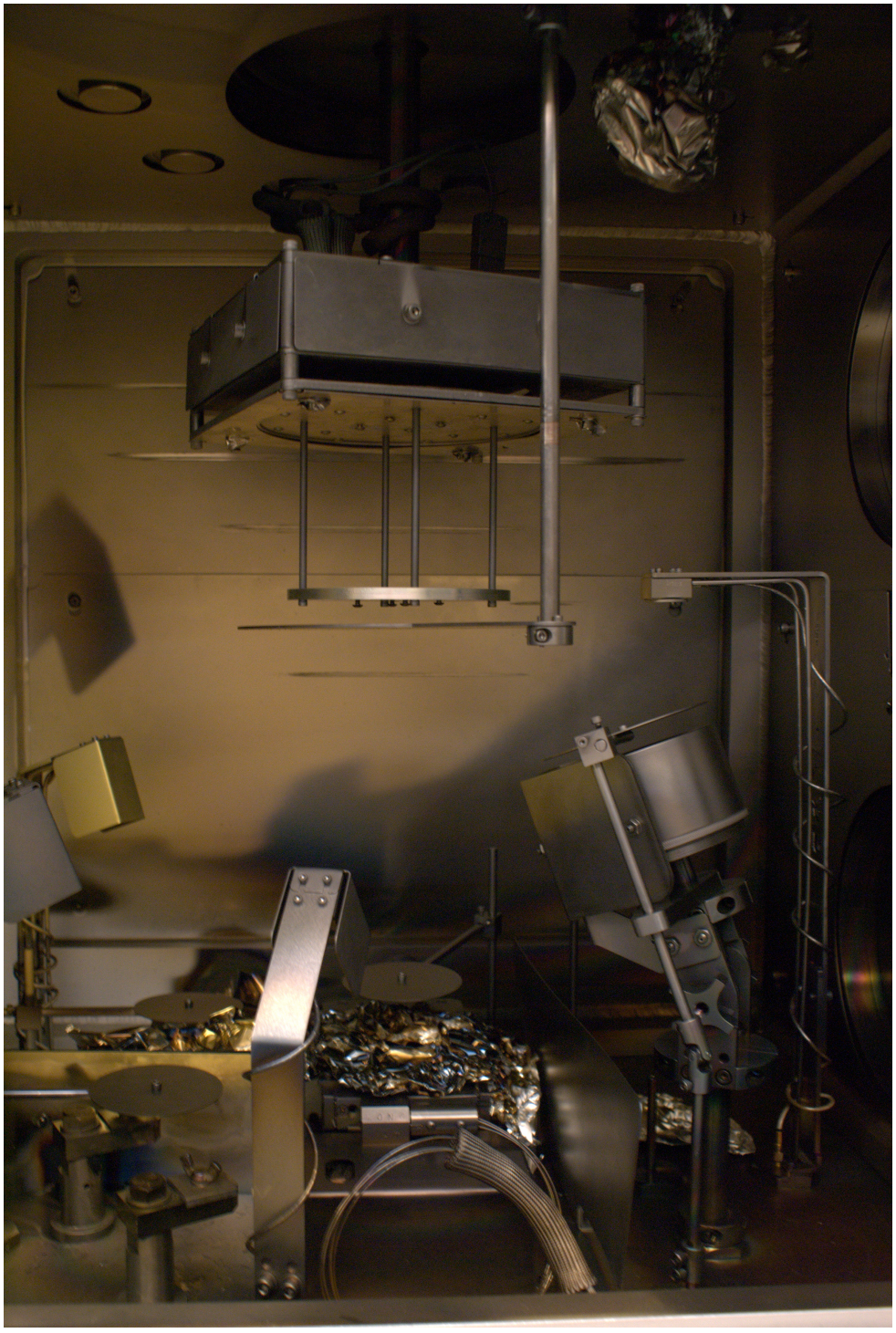

Figure 4.1: The inside of the Angstrom system at the MORE center. The added smaple mount is seen hanging from the original mount by 4" supports. The e-beam PVD pocket is located firectly below the sample mounts and the surviving DC sputtering assembly is seen on the left.

material on each side and variation of any kind would disrupt the periodicity of the crystal that is fundamental to its function.

4.1.1 Electron Beam PVD

Materials that can be bought commercially as pellets and that vaporize upon heating with an electron beam are ideally deposited using e-beam PVD. Silica happens to be one such material as it is readily available as 99.99% pure amorphous pellets from International Advanced Materials. The process of vaporizing the silica is complicated by the fact that it does not create a melt and a direct application of the electron beam would burn through the ceramic vessel containing it and into the instrument itself. To counter this potential hazard we sweep the silica pocket in a circular fashion. We optimize the sweep to cover a maximal amount of area by adjusting the movement of the beam using a joystick-like interface and monitoring the beam through a window on the front of the system. Furthermore, we maintain at least a $\frac{3}{4}$ filling of the crucible so as to refrain from hitting it with the electron beam, which would inevitably crack the crucible and cause a malfunction.

Once the silica has been excited enough to maintain a steady vaporization the entire chamber is flooded with its particles, including the target whose thickness is monitored by a dedicated quartz crystal. Using a parameter called the tooling factor we can set a final thickness and the system will determine the time necessary to complete the deposition and shut itself off. The tooling factor is defined as $TF = \frac{actual}{desired} * 100\%$ which merely states that it is a proportionality that the quartz crystal is to account for when depositing a specified material. A calibration for the tooling factor is done regularly (weekly) and the quartz crystals are replaced once their lifetime is around 60% as consistent deposition of

oxide materials degrades them more rapidly than non-oxide materials. Compounding the volume of users that frequent the MORE center and use the Angstrom system this results in the quartz crystal monitoring the e-beam PVD pocket being changed approximately once a month.

4.1.2 Magnetron Sputtering

Titania, which is not available in pellet form is instead deposited using RF magnetron sputtering. In this case we have a plate of 99.98% pure titania, purchased from Stanford Materials, that is held in place by concentric rings that attach it to electrodes. The chamber is flooded with 15ppm of argon and a radio frequency is sent through the electrodes to ignite a plasma above the target which ionizes the argon particles in its vicinity. Once the plasma was ignited the argon was reduced to a partial pressure of 5ppm which allows each ion to become more energized and thus ease the sputtering process. The ions are guided toward the target by magnets, hence the magnetron component of the name, and impact the titania plate with a large amount of kinetic energy. This energy is used to dislodge titania particles that then flood the chamber and deposit on the suspended substrate. Again, we wish to deposit the titania with high accuracy and precision but due to our modifications, described in the Challenges section, the tooling factor is insufficient. As such we run the machine manually meaning that we deposit for a specified time and then measure the thickness using a stylus profilometer. This is repeated for a series of times at ten minute intervals to generate a calibration curve again shown in the Challenges section.

4.1.3 Spin Coating

The final component to our optical cavity is the defect layer containing the embedded quantum dots. We hoped to achieve the embedding of the quantum dots by dispersing them in polysilazane and spin-coating them on a the defect silica layer. The process of spin-coating is rather simple: A substrate is held in place by a vacuum on a pedestal which rotates at very high speeds, up to 9000rpm, while we drop our dispersion on its center. This rapid rotation allows for a homogeneous coating of the substrate provided that it is symmetric, which is true in the case of our 1cm square quartz slides that will be used for the final product. The quartz test slides are rectangular and spin-coating these results in a radial distribution equal to the width of the slide.

4.2 Challenges

During the course of experimentation with the Angstrom system we encountered two major problems:

1. The time it took to deposit the titania using RF magnetron sputtering was not feasible for our restricted means

2. The usual supplier of polysilazane cited in literature for this sort of application sold its patent to a company that was much less willing to sell to us

First, using the sputtering assembly it took about one-and-half hours to deposit 25nm of material. Given that we need to repeat this twenty-eight times at a thickness of 64nm and that the machine can be reserved for at most four hours this was not a viable approach. To overcome this problem three strategies were devised and attempted before we finally decided to design and build a new support that would reduce the separation

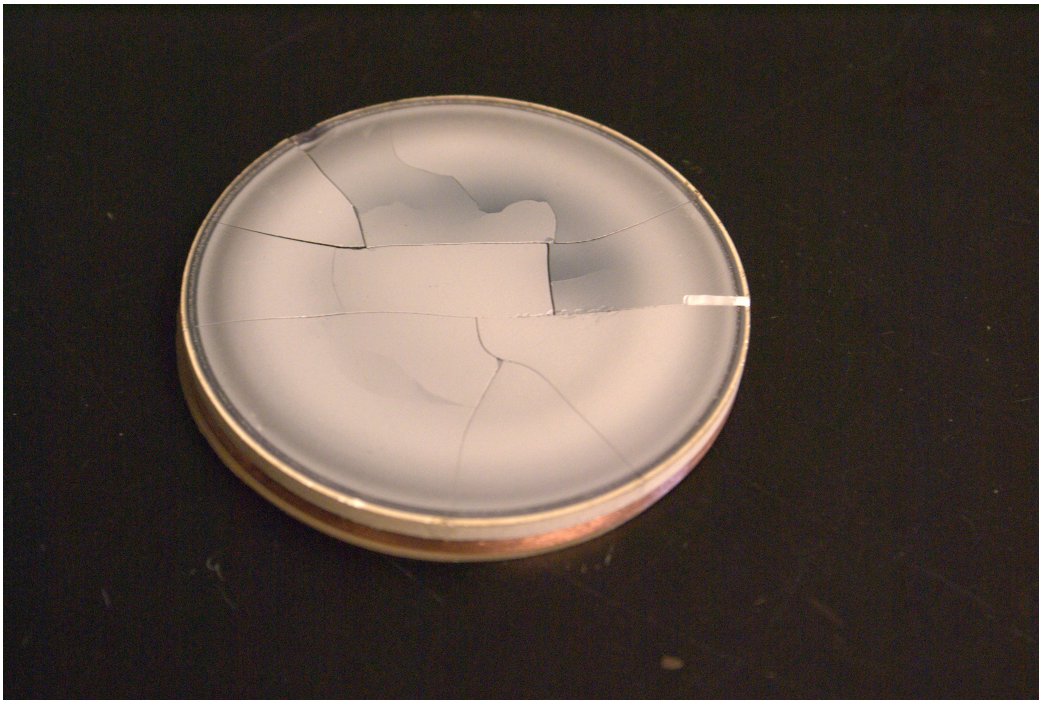

Figure 4.2: Cracked titania plate. Note the darker region which resulted from a plasma arc on one of the runs that went above 30% power.

of the substrate and target by four inches. The first of these strategies was to increase the power of the radio frequency, which proved to be damaging for the TiO_2 plate above 30% of its maximum value of 600W. Apparently, the plate was excited to a point that the resulting vibrations severed the crystal structure and created a crack across its entirety. Recouping from the damage we summarily ceased testing the target above 30% and opted to try the deposition using the other sputtering assembly available, one that applies a direct current.

This proved to be even slower than the RF process despite being able to run at a higher power, 400W, and was also scraped as a possible solution. Ultimately we opted to build a new substrate holder that is identical to the old one save for the fact that it is four inches lower, reducing the target to substrate distance to five inches. The new sample holder attaches to the old one using four beams and though it is smaller in diameter

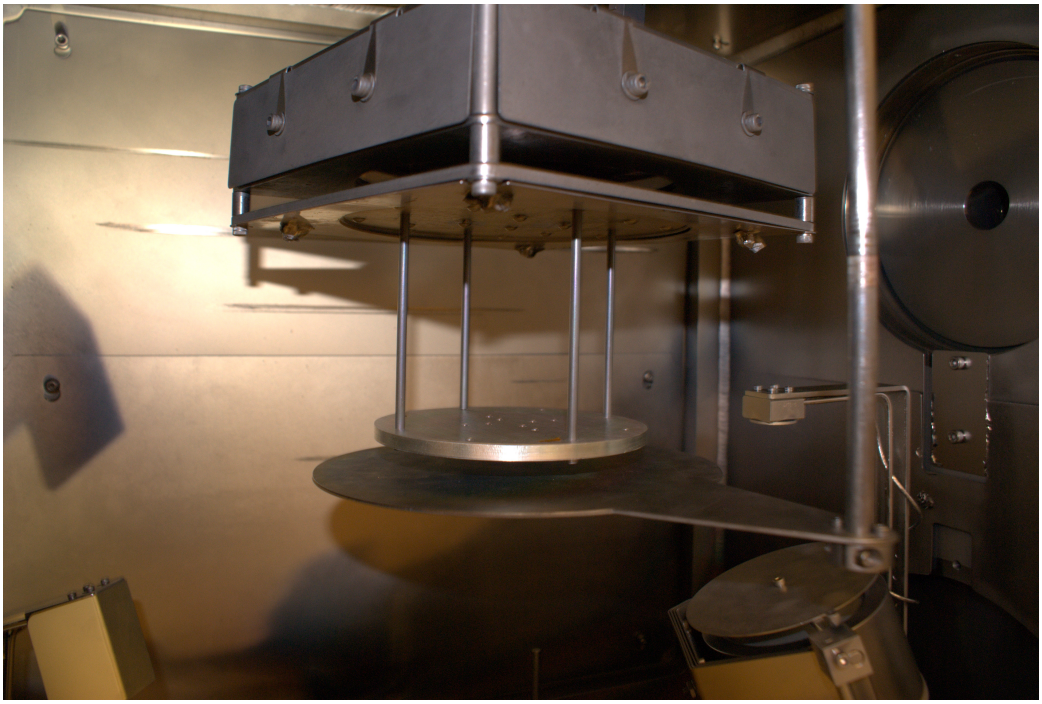

Figure 4.3: Close-up picture of the secondary sample mount that was fabricated.

still allows for three slides to be loaded at a time. It was hypothesized that this would improve performance proportional to the square of the distance, i.e. 16-fold, whereas we saw an actual six-fold reduction in deposition time. Now, we are able to deposit 60nm of titania in half an hour and 100nm of silica in about ten minutes. This then makes it feasible to deposit multiple stacks during a single reservation as well as helping other groups that use the machine and have experienced similar problems.

The model for our cavity was inspired by Senellart et. al. in which the use polysilazane to embed quantum dots in the defect layer of the cavity. [2] In their letter, received in 2005, they state that the polysilazane was purchased form Clariant Ltd., a commonly known international chemical supplier. However, in 2011 Clariant chose not to renew their patent and instead sold it to AZ Electronic Materials which has upgraded the product line to feature a number of polysilazanes with catalysts and optional functionalities. The standard perhydropolysilazane that we would use is included in their product line as

SpinFil100, however they were reluctant to sell when approached. After a series of e-mail communications they expressed their willingness to cooperate on the condition that we schedule conference calls and file a non-disclosure agreement (NDA). This proved to be a tedious process and eventually we opted to pass them on, instead beginning talks with KiON, another supplier of polysilazane in the U.S.A. KiON did not require a NDA but they refused to sell on the grounds that they are part of the department of defense and cannot sell to non-military personnel. As a result we chose to revise the plan for embedding the quantum dots in such a way that would not require polysilazane. The new approach would use either a paste or viscous solvent in which the QD's would be dispersed and then spin-coated in the same fashion. This would however require further testing on the part of the experimenter to determine which solvents gave the most homogeneous dispersion of QD's, at what speeds, and in what density.

4.3 Characterization and Profiling

Along with knowing the thickness of the layers that we deposit it is important to determine their optical properties, namely the refractive index. To this end we employ a KLA Tencor P-6 stylus profilometer equipped with a 2 micron diamond stylus and a Horiba Jabin Yvon UviSel spectroscopic ellipsometer.

In order to measure the thickness of a sample we have to create a step which is achieved by covering a small section of our sample with a piece of tape. After deposition is complete we can remove this tape and pass the stylus across the edge left behind. For individual layers the contrast is very low but this is mitigated by a optical microscope that is attached to the profilometer, so aligning the tip is a simple matter.

To determine the refractive index of our layers we collect reflection data using ellip-

sometry and fit it to existing theoretical models for the materials we wish to characterize that are found in the program's library. In our case we fit data to amorphous silica and titania and we account for the interfaces using a specially defined "void" layer. The data is collected as the change in polarization of light as it is reflected from our surface. By increasing the gain on the instrument we can optimize our resolution and obtain data on multiple layers at a time, given that we have calibrated it for individual layers and the substrate beforehand.

Chapter 5

Discussion

At its conclusion the project has been carried through three of the four initial objectives laid out in the Introduction. This is a slight overstatement as the cavity itself has not been built nor have we been able to incorporate the QD's into the defect layer. The final objective, which relies on the full completion of the first three, is incomplete for obvious reasons. What follows is a thorough discussion on the objectives in the order that they appear at the beginning of this paper.

The first objective is above all the most complete of the set. We have successfully used MEEP to simulate our cavity, specifically for the purpose of optimizing construction. The quality factor has been determined for various numbers of stacks but we have been unable to reproduce the transmission spectrum that was obtained from the TM program. The cause of this discrepancy, that a mode of 600nm was found yet was not observed on the transmission spectrum, is unknown. Possible causes include the size of sources that we use, perhaps they have to be closer, more intense, or larger so as to cover the surface of the structure. Another possibility is that the use of the functions *infinity* or *no-size* is limiting the simulation. This can be tested by scripting the structure in three

dimensions, a more time-consuming objective than difficult. A simple simulation in three dimensions of one stack shows no difference in behavior from that in two dimensions so this resolution is highly speculative.

In the case of the second objective there has been a great deal of challenge and bureaucratic impedance. First, we encountered unreasonable deposition times with respect to titania and this required considerable troubleshooting before the solution was "brute-forced" in the form of a new substrate mount. Following this was a long period of calibration for the new support which negated the use of the preprogrammed tooling factor. Finally, we were unable to obtain polysilazane from two different vendors and have decided to forgo that approach hoping to replace it with a less complicated method. The actual construction of the cavity had begun in late March, 2013 but then in the first week of April the cooling lines of the RF sputtering assembly experienced a catastrophic leak. The entire system had to be disassembled, all the control instruments tested individually, and the sputtering arm sent back to the manufacturer. To the date of this paper's writing the arm has not been returned to the MORE center and production has ceased.

The third objective is about as complete as the first. Ellipsometry and profilometry have been conducted on individual layers and compound stacks, but the objective is vague enough to include a final characterization and thus is not fulfilled. In terms of the fourth objective there is not much to say. The experimental setup is within the Berezovsky lab but since we are lacking a cavity to test we cannot possibly hope to carry out the experiment at this time.

Chapter 6

Conclusion & Future Outlook

The project has led to a number of success and is concluded with a hopeful outlook on its continuation. The secondary support that was built has increased efficiency in silica and titania depositions by six-fold and has been calibrated to do so with 5% and 8% accuracy, respectively. Simulations in both one and two dimensions have been done with MEEP leading to an optimization of cavity design through harmonic analyses of quality factor at $Q \approx 2000$ with fourteen stacks. This structure was then verified with transfer matrix calculations which showed the stop-band and resonance characteristics that were expected.

Moving forward it is necessary to design and optimize a spin-coating method for the QD's that doesn't utilize polysilazane. The difficulty here lies not with the deposition as they will still be embedded but with the degree of dispersion that various solvents will afford. Since the Angstrom system is calibrated once it is fully repaired it can be run for the approximate 14 hours that it will now take to deposit one side of the cavity.

Chapter 7

Acknowledgments

First and foremost I would like to thank Dr's. Berezovsky, Petschek, and Singer, who have advised me throughout my senior project. A special thank you goes out to Jesse Berezovsky for his invitation to do a project under his tutelage and assistance in understanding the theory and motivations behind it. Among peers I would like to thank Ahmad Khastehdel and Rosemary Bramante in aiding me fabricate the secondary support and code the transfer matrix calculations. This project would not have been possible without the MORE center and its director Dr. Ina Martin who keeps it running at top performance and has taught me a great deal about administering the lab as well as about the inner workings of the instruments contained therein. Along the way I had many of my questions answered by various faculty members of the Physics Department with whom I have had the pleasure of spending the last four years of my academic career.

Bibliography

[1] Reitzenstein, S. *J. Selected Topics in Quantum Electronics* **2012**, 18(6), 1733-1746.

[2] Peter, E.; Senellart, D.; Martrou, D. *Physical Review Letters* **2005**, 95, 67401.

[3] Kahl, M.; Thomay, T.; Kohnle, V. *Nano Letters* **2007**, 7(9), 2897-2900.

[4] Gerard; J. M.; Sermage, B.; Gayral, B. *Physical Review Letters* **1998**, 81(5), 1110-1113.

[5] John D. Joannopoulos, Steven G. Johnson, Joshua N. Winn, Robert D. Meade, *Photonic Crystals: Molding the Flow of Light*, **2008**, (New Jersey: Princeton Press), 44-65.

[6] Pochi Yeh, *Optical Waves in Layered Media*, **1988**, (New York: Wiley).

[7] Vahala, K. J. *Optical Microcavities*, *Nature*, **2003**, 424, 839-846.

[8] Fermi, E. *Reviews of Modern Physics*, **1932**, 4, 87-132.

[9] Jaynes, E. T.; Cummings, F. W. *Proceedings of the IEEE*, **1962**, 89-109.

[10] Haroche, S.; Kleppner, D. *Phys. Today*, **1989**, 42(1), 24-30.

[11] Fowles, G. R. *Introduction to Modern Optics*, **1975**, (New York: Dover), 189-193.